Influence of star-like iridium complexes in the graphoepitaxy of polyfluorene thin films

M. Knaapila,[1,*] M. Torkkeli,[2] B. P. Lyons,[1,†] M. R. C. Hunt,[1] T. P. A. Hase,[1] O. H. Seeck,[3] L. Bouchenoire,[4] R. Serimaa,[2] and A. P. Monkman[1]

[1]*Department of Physics, University of Durham, South Road, Durham DH1 3LE, United Kindom*

[2]*Department of Physical Sciences, University of Helsinki, P.O. Box 64, FI-00014, Finland*

[3]*HASYLAB am DESY, Notkestrasse 85, D-22605 Hamburg, Germany*

[4]*XMaS, European Synchrotron Radiation Facility, Boîte Postale 220, F-38043, Grenoble Cedex 9, France*

(Received 8 May 2006; revised manuscript received 21 October 2006; published 18 December 2006)

We report on the impact on the equatorial and meridional orientation in hairy-rod poly[9,9-bis(2-ethylhexyl)-fluorene-2,7-diyl] thin films when blended with tris-cyclometalated oligo-fluorenylpyridine iridium(III) complex. The presence of this transition-metal complex does not alter the underlying helical motif of the polymer chain or the hexagonal unit-cell intermolecular packing. However, systematic changes in the resulting texture patterning of the crystallites are observed. Crystallites with two preferred *a*-*b* orientations, so called type I and II and differing by 30 degrees, are superimposed on an isotropic background that is designated as type III. The extent of meridional alignment for all three is found to be similar.

DOI: 10.1103/PhysRevB.74.214203 PACS number(s): 61.10.−i, 82.35.Lr, 81.07.Bc, 81.16.Dn

Manipulating and controlling the molecular-level structure of functionalized polymers in bulk and at surfaces is central to the science and applications of these materials. Hairy-rod polymers[1] are one important example and, among those with π-conjugated backbones[2] [e.g., poly(*p*-phenylenes),[3] polyfluorenes (PFs),[4] and ladder derivatives[5]], the nature of the main chain conformation and interchain packing are crucial factors in ultimately determining optical and transport properties. The structural characteristics at larger length scales are equally as important, and this has been the main emphasis in a number of recent studies. A classic example is the poly(3-alkylthiophene) family[6] in which the extent of structural isomorphism or regioregularity strongly affects the internal crystallite structure[7] and the subsequent structural evolution when intercalated or doped.[8]

Among PFs, important blue emitting polymers, even small differences in the molecular structure can influence the charge carrier mobility[9] and fluorescence.[10] Poly[9,9-bis(2-ethylhexyl)-9H-fluorene-2,7-diyl] (or PF2/6) (Ref. 11) is a well-known helical PF polymer functionalized with branched alkyl side chains. PF2/6's optical properties[12] are relatively insensitive to either changes in the molecular weight (MW) or processing history, and so it is an excellent model system for studies of intermolecular self-organization.[13] However, this intermolecular assembly is affected by changes in the MW (or number averaged MW, M_n). In PF2/6, there is a threshold MW, M_n^*, at which there is a crossover in the phase behavior.[14] Low MW samples exhibit only a single nematic liquid crystal phase (*n*-LC and $M_n < M_n^*$) while high MW samples ($M_n > M_n^*$) include a distinctive thermotropic transition between this *n*-LC phase and a hexagonal crystalline phase. This threshold MW also marks sharp changes in both meridional alignment[15] and surface morphology.[16] In aligned films on rubbed polyimide (PI), the rigid PF2/6 lies on the substrate with the helical axes pointing along the rubbing direction (denoted **z** here). Consequently, meridional alignment leads to a large absorption and dispersion of the refractive index in the (*xy*0) plane along the **z** axis.[17] The aligned films show two different *equatorially* oriented coexisting crystallite types in-plane.[18] Type I has its crystal axis **a** normal to the surface (**x**) and type II along the substrate surface (**y**). The differently oriented crystallite types are present both in uniaxially aligned and in-plane aligned films.[15] This indicates that (macroscopic) meridional and (surface preferential) equatorial alignment of PF2/6 crystallites are two distinct processes. PF2/6 has potential in thin-film device applications as a white light emitting diode made via "doping" with rubrene[19] or star-like tris-cyclometalated oligo-fluorenylpyridine iridium(III) [$Ir(Fl_xPy)_3$] guests.[20,21] If polarized white emitters of high charger mobility, achieved via alignment, are desired, it is important to understand how these guest molecules perturb alignment and crystallite orientation.

To date, the crystallite orientation has been studied only in pure PF2/6,[18] and therefore there is an interest to extend this work for the host-guest system. The ultimate question is whether guest molecules tune the equatorial crystallite orientation while still maintaining a reasonable degree of meridional orientation. In this paper, we have studied PF2/6 mixed with an $Ir(Fl_xPy)_3$ guest and we describe how the meridionally aligned PF2/6-$Ir(Fl_xPy)_3$ system differs from pure PF2/6 in the vicinity of M_n^* where the degree of uniaxial alignment of PF2/6 is maximized. The degree of meridional alignment of the PF2/6-$Ir(Fl_xPy)_3$ system near M_n^* does not decrease, when $x=1$ or 3 or when 1 wt. % guest is used, but decreases slightly when 5 wt. % $Ir(Fl_5Py)_3$ is used. The focus has been on the case $M_n > M_n^*$.

The preparation of PF2/6 (Ref. 22) and $Ir(F1_xPy)_3$ ($x=1,3$, or 5) (Ref. 21) (Fig. 1) have been described elsewhere. 8/15-PF2/6 with phenyl and 29/68-PF2/6 with an *N*-di(4-methyl-phenyl)aminophenyl end-cap were used. The prefix denotes molecular weights M_n/M_w in kg/mol. The polymers were dissolved in a 3:1 mixture of toluene and chloroform (Aldrich). Samples were made by spin-coating from 10 mg/mL solutions at 2500 rpm for 60 s under clean room conditions. To align the PF2/6 films, the samples were annealed in the nematic state at 180 °C (under vacuum) on rubbed PI as described in Refs. 14 and 15. In the film geom-

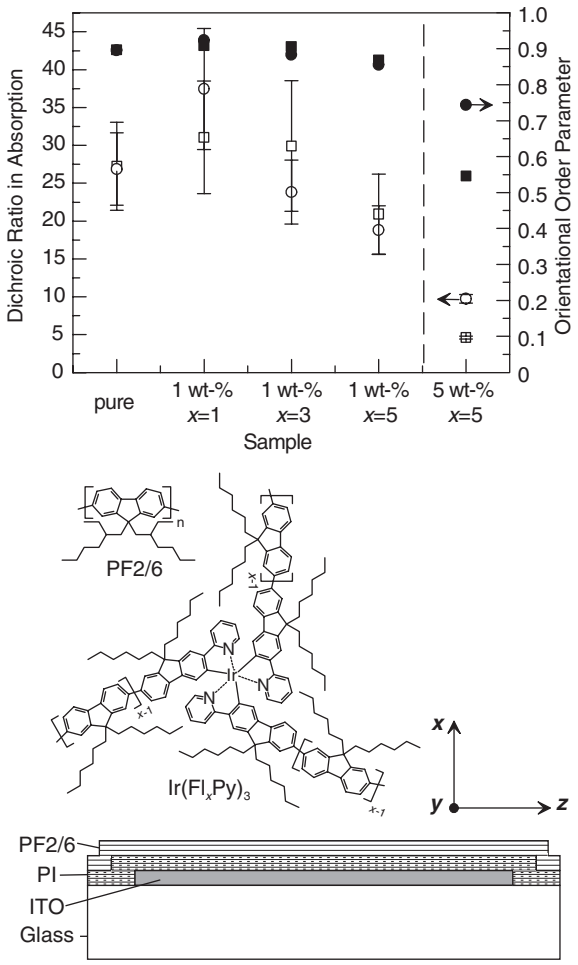

FIG. 1. Above: Dichroic ratio (open symbols) and order parameter s (solid symbols) of nematic 8/15-PF2/6 (squares) and hexagonal 29/68-PF2/6 (circles) with Ir(Fl$_x$Py)$_3$, (x=1, 3, or 5) complex. Below: Schematics of PF2/6, Ir(Fl$_x$Py)$_3$ (x=1,3,5), and an experimental geometry. ϕ is the angle between the incident beam and **z** axis in the (0yz) plane.

etry, the **x** axis is defined normal to the surface while **y** and **z** axes are parallel to the surface with **z** coinciding with the alignment direction (Fig. 1). Meridional and equatorial refer to the **z** axis and (xy0) plane, respectively. Films were stored in the dark and kept under inert gas during the measurements.

The synthesis of Ir(Fl$_x$Py)$_3$ involves heating up to 200 °C, at which temperature the thermogravimetric analysis (TGA) of Ir(Fl$_x$Py)$_3$ does not indicate any major loss of mass. The alignment involves heating up to 180 °C (in argon), and PF2/6 (Ref. 14) and oligofluorenes[23] are found to be stable up to ~300 °C. Thus we assume that the studied materials are not degraded during the alignment process.

TGA and polarized absorption measurements, respectively, were performed as detailed in Refs. 14 and 15. The dichroic ratio is given by $R=|\bar{E}_{\parallel}/\bar{E}_{\perp}|$; $\bar{E}_{\parallel}$ and $\bar{E}_{\perp}$, respectively, are the maximum values of the absorbance for light polarized parallel to **z** and **y** axes. The order parameter is $s=(R-1)/(R+2)$.

Grazing-incidence x-ray diffraction (GIXD) measurements were performed at the W1.1 (ROEWI) beam line at HASYLAB in Hamburg (Germany). The beam [10.5 keV, 0.2×2 mm(vert.×hor.)] was monochromatized by a double crystal Si(111) monochromator and focused on the sample. A helium atmosphere was used. The incident angle (0.11°) was below the critical angle of PF2/6. The GIXD patterns were measured with the incident beam along the **z** and **y** axes, respectively. The 1D intensity was measured with a scintillation counter and 2D intensity with an image plate (Molecular Dynamics), and for normalization, the incident flux was measured with an ionization chamber. The instrumental function was found to be negligible. The phi scans [the angle between the incident beam and **z** axis in the (0yz) plane] were performed at the XMaS beamline[24] at the ESRF (France) using a similar GIXD geometry, beam size, and incident angle as at HASYLAB. The GIXD data were measured using a MarCCD detector and normalized using an ionization chamber. As the measured scattering patterns do not change during the phi scans, no substantial radiation damage occurred. The peak broadening was studied as outlined in Refs. 14 and 15.

Atomic force microscopy (AFM) was performed in noncontact mode using an ultrahigh-vacuum scanned probe microscope (Omicron VT-SPM) operating at room temperature and a pressure of 1.1×10^{-10} mbar. Samples previously examined by GIXD were directly mounted onto standard sample spades using conductive tape and imaged without any further preparation. All the images have been subjected to a third-order average plane subtraction, but are otherwise unprocessed.

The degree of meridional alignment is greatest near M_n^* (Ref. 15) and therefore the alignment of a sample slightly below and above the nematic-hexagonal phase transition[14] was studied using polarized absorption. Nematic 8/15-PF2/6 and hexagonal 29/68-PF2/6 were selected. Both PF2/6 and Ir(Fl$_x$Py)$_3$ consist of fluorene units, so all absorption spectra and emission profile (measured at 440 and 570 nm) of our samples are typical for PF2/6 with the maximum at 370–380 nm.

Figure 1 shows the dichroic ratio in absorption (R) and orientational order parameter (s) of pure and doped samples (see definitions above). Pure 8/15-PF2/6 and 29/68-PF2/6 are observed to align equally well. When the materials are doped by 1 wt. % of Ir(Fl$_x$Py)$_3$, no essential difference between 8/15-PF2/6 and 29/68-PF2/6 is seen, but the degree of alignment tends to decrease with increased side chain length of the Ir(Fl$_x$Py)$_3$ but still remains high. Unsurprisingly, the bulkiest guest, Ir(Fl$_5$Py)$_3$ has the largest effect on the meridional orientation of both nematic and hexagonal PF2/6. At 5 wt. % of Ir(Fl$_5$Py)$_3$, R drops by a factor of 2 and 29/68-PF2/6 shows higher value over 8/15-PF2/6. As we observe lower fluorescence anisotropy for doped samples, the difference in absorption is due to diminished meridional alignment of the doped samples, rather than an isotropic guest background.

The shape of the polarized PL spectra remains unchanged upon doping by Ir(Fl$_x$Py)$_3$. Light emission from the doped sample is less polarized and we do not observe any effect of dopant or emission from the dopant. There is poor overlap

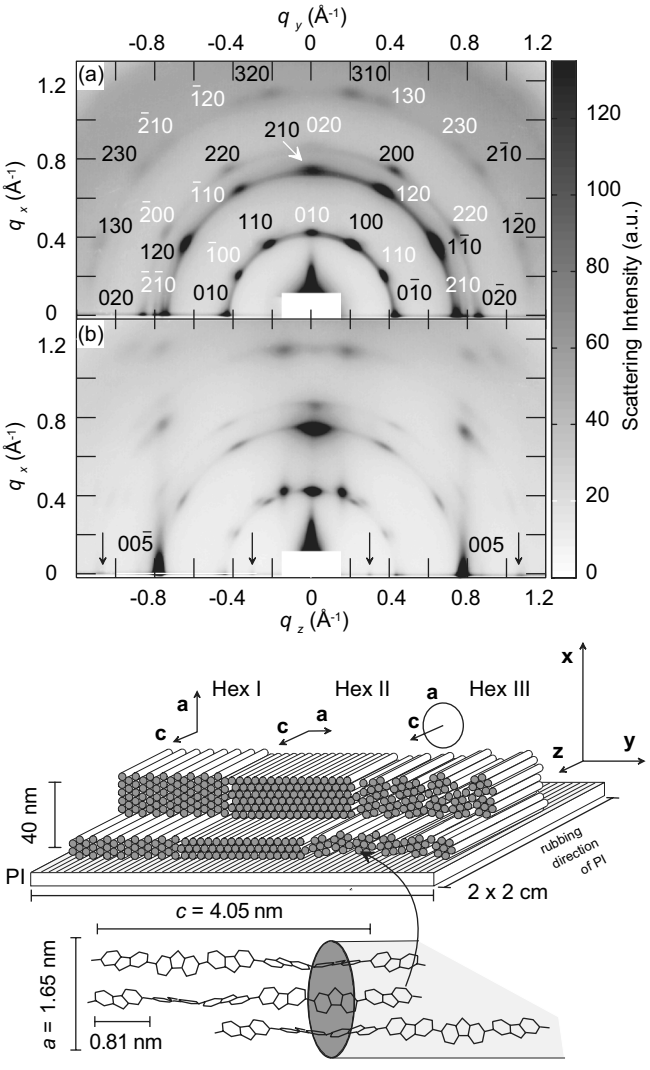

FIG. 2. Above: GIXD patterns of 5 wt. % $Ir(Fl_5Py)_3$ doped 29/68-PF2/6. (a) ($xy0$) plane. (b) ($x0z$) plane. The GIXD patterns were measured with the incident beam along the **z** and **y** axes, respectively. Black and white indices show the primary reflections of the types I and II, respectively. Type III appears as diffraction arcs. Below: Schematics of the proposed arrangement of crystallite types I–III.

between dopant absorption and host emission, and so no Förster transfer occurs in this case.

$Ir(Fl_5Py)_3$, which most influences the alignment in the ($00c$) plane (cf. Fig. 1), was expected to reveal the largest effect on the local structure. For that reason we shall limit our discussion to this sample alone.

As described in our previous publication[15], pure 29/68-PF2/6 shows two hexagonal GIXD patterns in the ($ab0$) plane rotated by 30° with respect to each other arising from types I and II. Pure $Ir(Fl_5Py)_3$ shows essentially one GIXD feature, a broad diffraction arc at 0.4 $Å^{-1}$, which we ascribe to the intermolecular distance between oligofluorene chains. However, the difference in GIXD patterns between 1 wt. % doped and pure material is small.

Figures 2(a) and 2(b) present the 2D GIXD patterns of 29/68-PF2/6 mixed by 5 wt. % $Ir(Fl_5Py)_3$ in the ($xy0$) and ($x0z$) planes, respectively. The GIXD patterns were measured with the incident beam along the **z** and **y** axes respectively. The reflections seen in Fig. 2(a) are in the ($xy0$) plane and those in Fig. 2(b) are at, or close to, the ($x0z$) plane. Note that the actual scattering vectors lie slightly off these planes. While the magnitude of the scattering vector is given by $q^2=q_x^2+q_y^2$, the tip of the q vector is rotated an angle $\text{asin}(q\lambda/4\pi)$ toward the reader. These reflections appear by virtue of a small in-plane spread in the **c** axis and out-of-plane spread in the **a** axis directions. Distinctive equatorial arcs appear in Fig. 2(a) alongside the peaks of types I and II crystallites. As the positions of the arcs agree with the q values of the hexagonal diffraction orders of pure PF2/6, they cannot arise from phase separated $Ir(Fl_5Py)_3$. Reflections of types I and II but no arcs are distinguishable in unaligned film on quartz,[15] and it is noteworthy that the arcs are not due to the decreased alignment along the ($00c$) direction but indicate hexagonal crystallites uniformly distributed on the ($ab0$) plane. The systematic reduction of uniaxial alignment, seen in Fig. 1 with increasing guest concentration, is paralleled by noticeable remnants of equatorial scattering not oriented with the rubbing direction. These features are clearly seen in the ($x0z$) plane in Fig. 2(b). The meridional scattering characteristics of the Five-fold helix remain unchanged. Therefore, we suggest that the arcs indicate a new hexagonal orientation type of PF2/6 in the ($ab0$) plane and call it type III. This axial texture relates closely to the classification of Heffelfinger and Burton.[25] The overall situation is illustrated in the scheme in Fig. 2.

Although $Ir(Fl_5Py)_3$ is a bulky molecule, any change (equatorial or meridional) in the lattice parameters of PF2/6 on doping is around 1%.[26] Therefore, $Ir(Fl_5Py)_3$ has essentially no influence on the intramolecular structure of PF2/6 or the intermolecular structure of crystallites. This result is in phenomenological accordance with the results of Prosa *et al.*[27] who reported that iodine intercalated poly(3-octylthiophene) shows several changes yet maintains the lamellar base structure of the pristine host when as much as 45 mol. wt. % iodine per octylthiophene monomer is added. We note, however, that in the latter the dopant is directly incorporated into the unit cell whereas here, in PF2/6, the additive seems to be inhomogeneously distributed and excluded from the crystallite core.

Examining Fig. 2(a) further, $Ir(Fl_5Py)_3$ seems to promote type II over type I. Based on the average intensities of the first-order reflections over the same azimuth angle (minus background), the fractions of types I, II, and III change from ~86%, ~14%, and 0% to ~36%, ~16%, and ~48% upon doping. Although we note that these absolute values can only give rough trends, the presence of the guest seems to interfere preferentially with the type I orientation.

Figure 2(b) shows reflections that are consistent with the usual 5-helix[11] but also a few extra reflections that do not conform to the 5-helix, marked by arrows. These weak reflections are present both in 29/68-PF2/6 (Ref. 16) and 5 wt. % $Ir(Fl_5Py)_3$ doped 29/68-PF2/6. These reflections are observed here as they are in fibre x-ray diffraction (XRD) patterns.[14] The peaks are likely related to the fact that the side chains of PF2/6 do not have the pure 5-helix symmetry of the genuine crystalline structure.

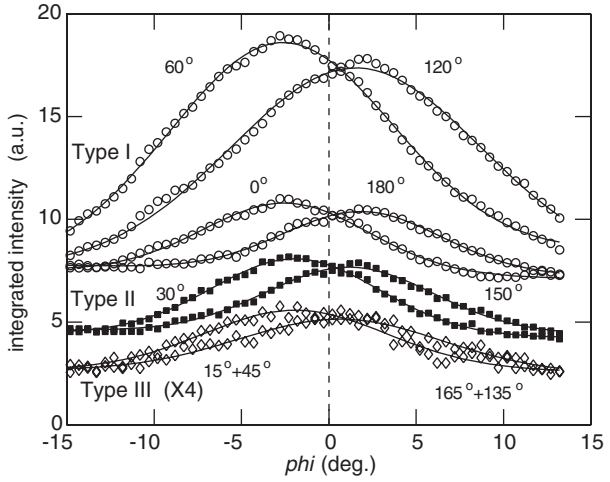

FIG. 3. Integrated intensities of the first hexagonal GIX reflections of 29/68-PF2/6 mixed by 5 wt. % $Ir(Fl_5Py)_3$. The sample is rotated about the **x** axis and ϕ is the angle between incident beam and **z** axis. Open spheres: Reflections 010, 110, 100, and $0\bar{1}0$ of type I. Solid squares: $\bar{1}00$ and 110 of type II. Open diamonds: arcs representing type III. This curve is multiplied by 4 for clarity. Labels denote clockwise rotation around the **z** axis (cf. Fig. 2). Solid lines are corresponding Gaussian fits.

Figure 3 plots the integrated intensities of the first hexagonal reflection ring as seen in Fig. 2(a) as a function of small azimuthal rotation ϕ of the sample around the **x** axis. All peaks show comparable distribution centered on the Bragg angle 2.05 degrees. Therefore, the degree of meridional alignment seems to be similar for all three crystallite types.

Upon doping, the equatorial crystallite size of types I and II drops from 35 to 23 nm. The difference between types is small whereas the crystallite size of type III in the (*ab*0) plane is further reduced (18 nm). On the other hand, these values are clearly of the same order of magnitude, which is in accord with the assumption that all the types I–III represent the same (local) structure but different (overall) alignment. In both doped and undoped samples, the meridional crystallite size is 35 nm. This value is obtained from the 005 reflections and one cannot distinguish here the different orientation types. These values are not much below typical film thicknesses (40–60 nm)[16]. In fiber XRD patterns of PF2/6,[14] the peak broadening of *hk*0 reflections scales as q^2 indicating paracrystalline order. However, in the doped case, the order approaches that of the genuine crystal. Flattening of unit cells along the **x** axis[18] probably caused by microstrains is also present and seen in small directional difference in peak positions.

The exact location of the iridium complex is not known, but because the lattice parameters are only weakly affected by the guest molecule, the guest is likely either micro- or macrophase separated. As type III domains are rich in voids at grain boundaries between the hexagonal crystallites, $Ir(Fl_5Py)_3$ might be in the voids in type III regions. A rigorous picture cannot be given at present, but if this picture is correct, it is unlikely that $Ir(Fl_5Py)_3$ can order like the polymer chains. In addition, dopant aggregation may be favored

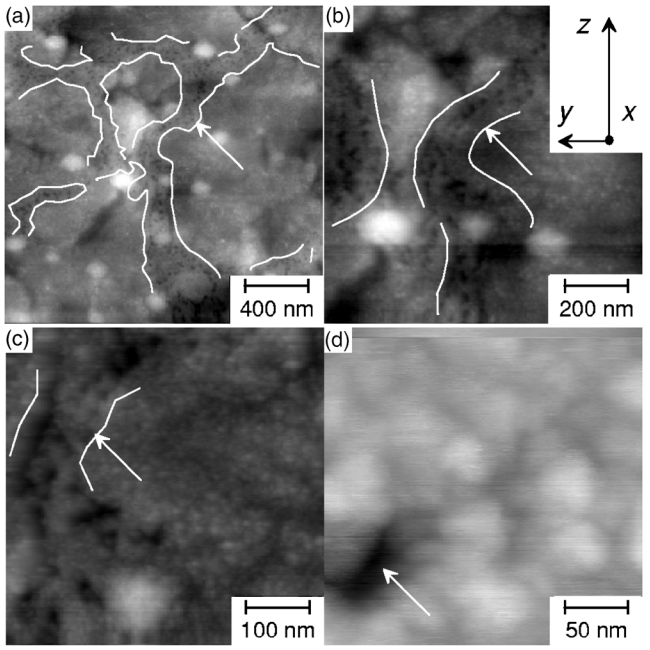

FIG. 4. Typical AFM images of 29/68-PF2/6 mixed by 5 wt. % $Ir(Fl_5Py)_3$. The height from black to white is (a) 30 nm, (b) 20 nm, (c) 15 nm, and (d) 5 nm. Inset shows the experimental geometry depicted in Figs. 1 and 2. Examples of areas rich in regular voids are marked by white lines and arrows.

at higher doping levels. The fact that there is poor Förster transfer to the dopant is consistent with the finding that the dopant is excluded from the PF2/6 crystallites. Förster transfer has a range of a few nanometers while the crystallite size is of the order of tens of nanometers. So many chains would be simply too far away from an iridium complex molecule.

The surface morphology of the samples and possible macrophase separation was studied using AFM. Figure 4 plots AFM images 29/68-PF2/6 mixed with 5 wt. % $Ir(Fl_5Py)_3$. As in the case of pure, similarly prepared 29/68-PF2/6 films[15], the surface of PF2/6-$Ir(Fl_5Py)_3$ is generally smooth with a typical roughness of the order of 2.6 nm as measured over a 1 μm $\times$ 1 μm area. However, attention is drawn to the long (>100 nm) areas containing voids of size 20–50 nm. These voids are not observed in the AFM images of pure 29/68-PF2/6. Their origin remains an open question. However, we note that the size of the domains in close proximity to the voids (width a few tens of nanometers) corresponds to the crystallite size of type III crystallites. These areas cover some tens of percent of the overall surface area of the sample, which is of the same order of magnitude as the fraction of the crystallite type III present calculated from the GIXD data. Therefore, this observation is in phenomenological agreement with the schematics shown in Fig. 2. These long areas seem to have a slight preference for alignment parallel to the **z** axis, but any tendency is small. We also observe regular features of size of 50–100 nm corresponding to the white areas in Figs. 4(a) and 4(b). As the fraction of these domains is of the same order as $Ir(Fl_5Py)_3$ fraction, this might be an indication of macrophase separation. However, there is no variation in the local (<50 nm) texture suggesting that the features are a natural variation of height rather

than any apparent macrophase separation, a conclusion that is consistent with the GIXD data

Summarizing, meridionally aligned PF2/6 shows changes in the nanocrystalline architecture when mixed with $Ir(Fl_xPy)_3$ guest in the vicinity of M_n^*. The results indicate that the inclusion of $Ir(Fl_xPy)_3$ does not interfere with the intramolecular helical or local hexagonal structure of the PF2/6 but has a role in nanoscale assembly of crystallites. In the (00*c*) direction, the degree of meridional orientation is preserved up to 5 wt. % $Ir(Fl_5Py)_3$. In the (*ab*0) plane, the PF2/6-$Ir(Fl_5Py)_3$ system shows crystallite types I and II that are rotated 30° with respect to each other and the surface plane, as in the aligned films of pure PF2/6, and a new orientation of crystallites denoted as type III that have no surface preference. The crystallite types are characterized by their orientation in the (*ab*0) plane and the hexagonal lattice parameters of PF2/6 remain essentially constant. As type III is rich in grain boundaries, the guest molecules can locate at those sites. No macrophase separation was observed. The degree of molecular alignment in the (00*c*) direction does not depend on the crystallite types. This suggests that the meridional alignment of the polymer rods and the equatorial alignment of crystallites are largely independent phenomena under the circumstances studied. In general, this work shows that a dye that is chemically compatible with a polymer matrix can cause a complicated change of the physical architecture of crystallites.

This study has been funded by One North-East UIC Nanotechnology Grant. We thank U. Scherf of the University of Wuppertal for polyfluorene, as well as M. Tavasli and M. R. Bryce of the University of Durham for the iridium complex. M.K. and M.T. thank DESY for support under Contract No. RII3-CT-2004-506008 (IA-SFS).

*Author to whom all correspondence should be addressed. Present address: MAX-lab, Lund University, P.O. Box 118, SE-22100 Lund, Sweden. Email address: matti.knaapila@maxlab.lu.se

†Present address: Institute of Materials Research and Engineering (IMRE), 3 Research Link, Singapore 117602.

[1] G. Wegner, Macromol. Chem. Phys. **204**, 347 (2003).

[2] T. Bjørnholm, T. Hassenkam, and N. Reitzel, J. Mater. Chem. **9**, 1975 (1999).

[3] S.-C. Yang, W. Graupner, S. Guha, P. Puschnig, C. Martin, H. R. Chandrasekhar, M. Chandrasekhar, G. Leising, C. Ambrosch-Draxl, and U. Scherf, Phys. Rev. Lett. **85**, 2388 (2000).

[4] W. Chunwaschirasiri, B. Tanto, D. L. Huber, and M. J. Winokur, Phys. Rev. Lett. **94**, 107402 (2005).

[5] W. Graupner, G. Leising, G. Lanzani, M. Nisoli, S. De Silvestri, and U. Scherf, Phys. Rev. Lett. **76**, 847 (1996).

[6] H. Sirringhaus, P. J. Brown, R. H. Friend, M. M. Nielsen, K. Bechgaard, B. M. W. Langeveld-Voss, A. J. H. Spiering, R. A. J. Janssen, E. W. Meijer, P. Herwig, and D. M. de Leeuw, Nature (London) **401**, 685 (1999).

[7] R. J. Kline and M. D. McGehee, J. Macromol. Sci., Polym. Rev 46, 27 (2006).

[8] G. Mao, M. J. Winokur, and F. E. Karasz, Phys. Rev. B **58**, 4089 (1998).

[9] C. L. Donley, J. Zaumseil, J. W. Andreasen, M. M. Nielsen, H. Sirringhaus, R. H. Friend, and J.-S. Kim, J. Am. Chem. Soc. **127**, 12890 (2005).

[10] K. Becker and J. M. Lupton, J. Am. Chem. Soc. **127**, 7306 (2005).

[11] G. Lieser, M. Oda, T. Miteva, A. Meisel, H.-G. Nothofer, U. Scherf, and D. Neher, Macromolecules **33**, 4490 (2000).

[12] S. Sinha, C. Rothe, R. Güntner, U. Scherf, and A. P. Monkman, Phys. Rev. Lett. **90**, 127402 (2003).

[13] M. Knaapila, R. Stepanyan, B. P. Lyons, M. Torkkeli, and A. P. Monkman, Adv. Funct. Mater. **16**, 599 (2006).

[14] M. Knaapila, R. Stepanyan, M. Torkkeli, B. P. Lyons, T. P. Ikonen, L. Almásy, J. P. Foreman, R. Serimaa, R. Güntner, U. Scherf, and A. P. Monkman, Phys. Rev. E **71**, 041802 (2005).

[15] M. Knaapila, R. Stepanyan, B. P. Lyons, M. Torkkeli, T. P. A. Hase, R. Serimaa, R. Güntner, O. H. Seeck, U. Scherf, and A. P. Monkman, Macromolecules **38**, 2744 (2005).

[16] M. Knaapila, B. P. Lyons, T. P. A. Hase, C. Pearson, M. C. Petty, L. Bouchenoire, P. Thompson, R. Serimaa, M. Torkkeli, and A. P. Monkman, Adv. Funct. Mater. **15**, 1517 (2005).

[17] B. P. Lyons and A. P. Monkman, J. Appl. Phys. **96**, 4735 (2004).

[18] M. Knaapila, B. P. Lyons, K. Kisko, J. P. Foreman, U. Vainio, M. Mihaylova, O. H. Seeck, L.-O. Pålsson, R. Serimaa, M. Torkkeli, and A. P. Monkman, J. Phys. Chem. B **107**, 12425 (2003).

[19] R. W. T. Higgins, A. P. Monkman, H.-G. Nothofer, and U. Scherf, Appl. Phys. Lett. **79**, 857 (2001).

[20] H. A. Al Attar, A. P. Monkman, M. Tavasli, S. Bettington, and M. R. Bryce, Appl. Phys. Lett. **86**, 121101 (2005).

[21] M. Tavasli, S. Bettington, M. R. Bryce, H. A. Al Attar, F. B. Dias, S. King, and A. P. Monkman, J. Mater. Chem. **15**, 4963 (2005).

[22] M. Grell, W. Knoll, D. Lupo, A. Meisel, T. Miteva, D. Neher, H.-G. Nothofer, U. Scherf, and A. Yasuda, Adv. Mater. (Weinheim, Ger.) **11**, 671 (1999).

[23] Y. Geng, A. Trajkovska, D. Katsis, J. J. Ou, S. W. Culligan, and S. H. Chen, J. Am. Chem. Soc. **124**, 8337 (2002).

[24] S. D. Brown, L. Bouchenoire, D. Bowyer, J. Kervin, D. Laundy, M. J. Longfield, D. Mannix, D. F. Paul, A. Stunault, P. Thompson, M. J. Cooper, C. A. Lucas, and W. G. Stirling, J. Synchrotron Radiat. **8**, 1172 (2001).

[25] C. J. Heffelfinger and R. L. Burton, J. Polym. Sci. **47**, 289 (1960).

[26] It should be noted that the precision of lattice parameters determined from experiments such as these is not high.

[27] T. J. Prosa, M. J. Winokur, J. Moulton, P. Smith, and A. J. Heeger, Phys. Rev. B **51**, 159 (1995).